Single-photon two-electron rearrangement transitions*

K. A. Jamison, J. M. Hall, J. Oltjen, C. W. Woods,† Robert L. Kauffman,‡
Tom J. Gray,§ and Patrick Richard
Department of Physics, Kansas State University, Manhattan, Kansas 66506
(Received 11 February 1976)

The observation and identification of K x rays resulting from one-photon two-electron rearrangement are made for Mg, Al, and Si following heavy-ion bombardment. Two types of rearrangement processes, which lead to K x rays below the energy of the characteristic $K\alpha$ x ray, are delineated: the radiative Auger effect (RAE) and radiative electron rearrangement (RER). The RAE process previously described by Åberg and Utriainen competes with the characteristic $K\alpha$ x ray. The observed energies and relative intensities RAE/$K\alpha$ from heavy-ion bombardment agree with those from electron and photon excitation. The RER process which we have recently proposed is the emission of a photon from the $(1s)^{-1}(2p)^{-n}$ to $(2s)^{-2}(2p)^{-n+1}$ electron rearrangement for $n = 1$–6. This model gives good agreement between measured and Hartree-Fock calculated RER energies. KL^n RER and $K\alpha L^n$ satellites are competing decay branches of the $(1s)^{-1}(2p)^{-n}$ initial configuration. The (KL^n RER)/$K\alpha L^n$ branching ratios are measured. The RER transitions are shown to be allowed by configuration mixing of final states with the same spin and parity. The branching ratio is a product of the mixing coefficient and a ratio of fluorescence yields. The theoretical branching ratios (KL^1 RER)/$K\alpha L^1$ and (KL^2 RER)/$K\alpha L^2$ are calculated and compared to experiment.

I. INTRODUCTION

In recent years there has been considerable interest in atomic transitions where multiple electron-vacancy rearrangements occur in atoms with one or more inner-shell vacancies. Of particular interest in this paper are processes in which more than one vacancy undergoes rearrangement and a single photon is emitted from an atom with a K-shell vacancy. Two types of single-photon two-electron rearrangement transitions are the radiative Auger effect[1,2] (RAE) and radiative electron rearrangement[3] (RER). In 1969, Åberg and Utriainen identified and reported the RAE in the K x-ray spectra of Mg, Al, Si, and S.[4] The RAE decay of a K-shell vacancy proceeds as a normal K Auger process, except that in addition to an electron filling the K vacancy and a second electron being ejected, there is also an emitted photon. The RAE produces a broad structure in K x-ray spectra less energetic than the characteristic $K\alpha_{1,2}$ x ray. The high-energy portion of the RAE structure exhibits a sharp edge corresponding to the ejected electron having zero velocity. The KL^2 RAE observed by Åberg and Utriainen[4] and the normal KL x-ray process are competing decay branches of the same initial state. This implies that the relative intensity of the KL^2 RAE and KL x ray should remain constant regardless of the method of producing the K-shell vacancy. The RAE was shown to be independent of the mode of excitation for e^- and photon excitation[5] and more recently for proton bombardment.[6]

A similar single-photon two-electron decay has been described as RER.[3] In this process a K x ray is emitted coincident with two $2s$ electrons undergoing rearrangement. One of the $2s$ electrons fills the K-shell vacancy, while the other is promoted to the $2p$ subshell. This process thus requires that in addition to the $1s$ vacancy there be at least one $2p$ vacancy present in the atom undergoing a RER transition. The lowest-energy RER is the transition from states with one $1s$ and one $2p$ vacancy. The addition of each L-shell vacancy increases the energy of the RER transition, so that an RER satellite sequence is predicted.[3] Four RER satellite peaks have been observed at x-ray energies between the RAE edge and the characteristic $K\alpha_{1,2}$ line. These peaks were first observed by Richard *et al.*[7] in 1973 with 30-MeV O bombardment and were reported with no definitive explanation. McWherter *et al.*[8] later suggested that these peaks were the result of multiple-volume plasmon excitation. The plasmon theory was shown to be inconsistent with the x-ray intensities observed with H and He bombardment.[3,9]

In this paper we report experimental results of the RAE and the RER single-photon two-electron rearrangement transitions resulting from heavy-ion bombardment. Initial measurements of RER branching ratios are also presented. A model for RER decay based on final-state configuration mixing is discussed. In this model multiplet states with the same spin and parity are mixed. Using this model we show that the branching ratio of the KL^n RER to the $K\alpha L^n$ x rays, originating from the initial configuration $(1s)^{-1}(2p)^{-n}$, is a product of a mixing coefficient and a fluorescence yield factor. The mixing coefficient is a function of the Slater exchange integral $G^1(2p2s)$ and the

observed KL^n RER to $K\alpha L_n$ energy splitting ϵ_n. The exchange integral is calculated using the Hartree-Fock program of Froese Fisher.[10] The fluorescence yield factor is calculated using partial multiplet fluorescence yields of Ne as given by Bhalla,[11] since the partial multiplet fluorescence yields of Mg, Al, and Si are not presently available. This may not introduce any significant error in the branching ratio, since the fluorescence yield factor is a ratio of partial multiplet fluorescence yields of a given configuration.

II. EXPERIMENTAL SETUP

A. Spectrometer

The experiment consisted of bombarding thick targets of Mg, Al, and Si with beams of H, He, C, N, O, F, and Cl ions at various energies from 0.4 to 2.3 MeV/amu. A four-inch curved crystal vacuum spectrometer was positioned at 90° with respect to the beam axis. Spectra were taken with the Rowland circle perpendicular to the beam axis as well as coplanar with the beam axis, and no appreciable change in the spectra was noted. Most of the data were taken in the perpendicular geometry. The beam current was integrated directly off the thick target and at each angular setting of the crystal the x-ray intensity was accumulated for a preset number of microcoulombs of beam current. Several different combinations of object and image slit widths were used, the most common being 0.011 in. object (crystal) slit and 0.010 in. image (proportional counter) slit. The flow mode proportional counter was equipped with a 2-μm Makrofol, used a P10 gas flow, and was operated at a bias of 2150 V.

B. H- and He-ion-beam measurements

The H- and He-ion beams were produced by the KSU single-stage AK-N Van de Graaff accelerator. Monoenergetic beams were momentum analyzed by a switching magnet and energy controlled by a fast-feedback slit control system. The beams were then focused by an electrostatic quadrupole to an approximately 2-mm beam spot and collimated to a 1.5-mm spot before hitting the target. Typical beam currents of 5–10 μA were used to scan the x-ray region of the RAE and RER transitions. This large current made it necessary to have a water-cooled target holder. A reduced beam current of ~100 nA was used to scan the x-ray region in the vicinity of the characteristic $K\alpha$ radiation in order to reduce pulse pileup and pulse-height defects in the proportional counter-preamplifier-amplifier system due to high count rates. The data were accumulated in a Nuclear Data 100 analyzer with multiscaling device allowing for variable spectrometer step size and variable integrated current per spectrometer step. The data were punched on paper tape for later off-line analysis on a PDP-15 computer.

C. Heavy-ion-beam measurements

Ion beams of C, N, O, F, and Cl were obtained from the KSU EN tandem Van de Graaff. Monoenergetic beams were focused with a magnetic quadrupole and collimated before hitting the target. Typical beam currents were on the order of 100–200 nA. Care was taken to insure that pileup did not occur in the $K\alpha$ satellite scanning region. Data taking was controlled by an on-line PDP computer through the multiscaler, as discussed in Sec. II B. The spectra were stored on magnetic tape for later off-line analysis.

D. Crystals

To ensure that the low-intensity peaks are not geometrical effects due to the crystal used in the spectrometer, several different crystals were used to observe this effect. Si x-ray spectra obtained with ammonium dihydrogen phosphate (ADP), pentaery thritol (PET), and ethylene diamine tartrate (EDdT) crystals gave the same results. All Si spectra reported in this paper were obtained with EDdT and PET crystals. The Al K x rays were analyzed with an ADP crystal. Mg spectra were obtained initially with a mica crystal in first order; however, much better energy resolution was obtained with a thallium ammonium phosphate (TlAP) crystal in second order. The consistent measurement of the RER peaks with four different curved crystals in first- and second-order x-ray spectra rules out any geometrical effects as the origin of these low-intensity peaks.

E. Data analysis

The energy calibration for each spectrum was based on the $K\alpha$ and $K\beta$ characteristic radiation and cross checked with the satellite energies available from heavy-ion bombardment.[12,13] A simple two-point linear calibration in wavelength provided the peak energies for the RER satellites and the RAE edge. The intensities of the $K\alpha L^n$ satellites were taken as the integrated intensity of each of the well-resolved peaks. The RAE intensity was taken as the integrated intensity below the RAE edge minus a background. The RER intensity was taken as the area of a Gaussian peak sitting on the background. The background was taken as a constant plus a Lorentzian tail due to the characteristic radiation. A best least-squares fit was made to each of the spectra, varying si-

multaneously the RER peak parameters and the background parameters. For the case of H- and He-ion data, a check was made to insure that the reduction in beam current provided a suitable normalization between the RER and characteristic radiation portions of the spectra where the beam current was much different.

III. EXPERIMENTAL RESULTS

A. Spectra

The initial motivation for doing this experiment was to verify that the RAE is independent of the mode of excitation.[6] This was accomplished by studying the K x-ray spectra of Mg, Al, and Si produced by heavy-ion impact. Figure 1 shows the results of Al bombarded with 1.5-MeV H. The structure between 1370 and 1400 eV is due to the RAE, with the ejected electron having very nearly zero energy and the photon having approximately the same energy as a $KL_{23}L_{23}$ Auger electron. The peak at 1406 eV has been identified[3] as the first line in a satellite sequence of KL^1 RER. KL^1 RER is an alternate decay branch of the $(1s)^{-1}(2p)^{-1}$ initial state competing with $K\alpha L^1$, which is the first satellite x-ray decay. Similar results for Si are shown in Fig. 2. The RAE edge is easily seen between 1600 and 1630 eV. Considerable structure whose origin is not fully understood is observed in this region. The first two RER peaks are visible at 1650.0 and 1666.3 eV (KL^1 RER and KL^2 RER). By comparing the Si and Al spectra one observes that the spacing between the RAE edge

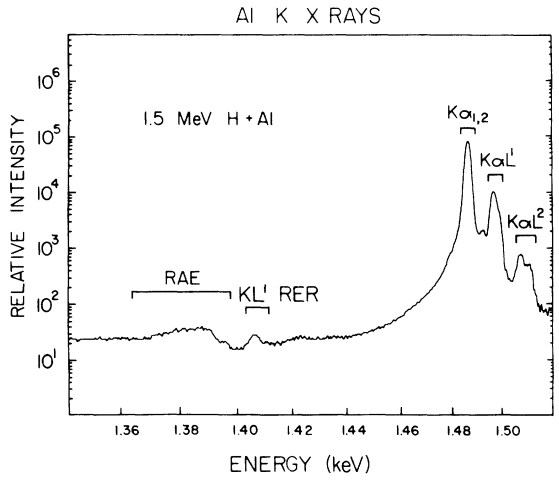

FIG. 1. Al K x-ray intensity as a function of energy in the region of $K\alpha_{1,2}$ as produced by 1.5-MeV H impact. The RAE edge is shown ~ 100 eV below the $K\alpha_{1,2}$ line and the first RER satellite is shown ~ 80 eV below $K\alpha_{1,2}$. These two-electron single-photon processes are several orders of magnitude less than the normal radiation.

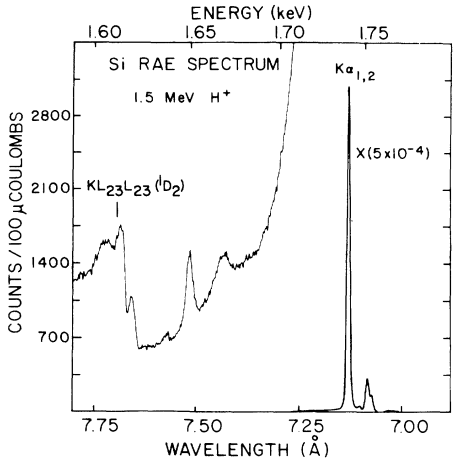

FIG. 2. Si K x-ray spectra analyzed in first order with an EDdT crystal. The RAE edge is clearly visible with 1.5-MeV H bombardment. Considerable structure is seen in the RAE region from 1600 to 1630 eV.

and KL^1 RER decreases dramatically as the target Z is lowered. Figure 3 shows that in the Mg K x-ray spectrum we are unable to resolve the RAE structure and the KL^1 RER peak. The RAE intensities for Mg, Al, and Si are approximately 0.002 of the intensity of the $K\alpha_{1,2}$ line. This is in agreement with the measurements for electron and photon bombardment.[2]

To enhance the RER satellite sequence it is necessary to produce more multiple L-shell vacancies concurrent with a K-shell vacancy in the atom. Figure 4 shows a spectrum obtained for Si bombardment by 2.4-MeV He. The peaks labeled KL^1 RER and KL^2 RER are enhanced nearly an

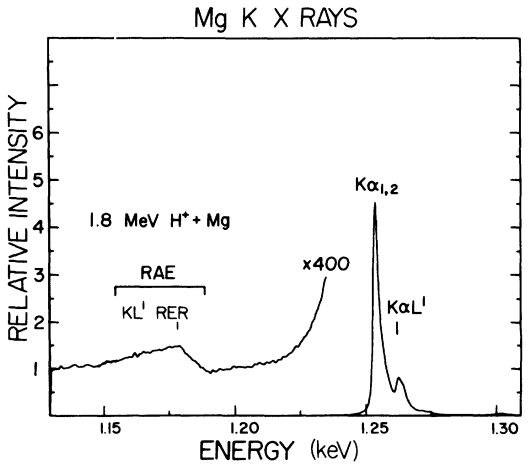

FIG. 3. Mg K x-ray intensity as a function of energy produced by 1.8-MeV H bombardment. The RAE edge and the first RER satellite are unresolved in this second-order TlAP crystal spectrum.

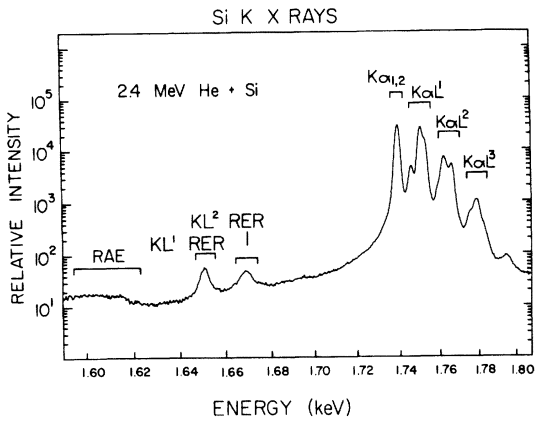

FIG. 4. 2.4-MeV He-produced Si K x rays as a function of energy. The increase in single-K multiple L-shell vacancy production as compared to H-induced spectra is noted to be coincident with an order-of-magnitude increase in the RER intensity for He bombardment compared to H impact.

order of magnitude relative to $K\alpha_{1,2}$ when compared to H-produced spectra. Coincident with the RER enhancement is the increase by an order of magnitude of the satellite peaks labeled $K\alpha L^1$ and $K\alpha L^2$. Since the intensities of both KL^1 RER and $K\alpha L^1$ increase an order of magnitude relative to $K\alpha_{1,2}$, the ratio of their intensities (branching ratio) remains approximately constant when the projectile is changed from H to He.

To further increase the amount of multiple L-shell ionization a variety of heavy-ion beams were used to produce the target x rays. Figure 5 shows the Al x-ray spectra produced by H, He, C, N, and O bombardment. The low-energy portion of each spectrum is magnified by an appropriate value to view the RAE and RER satellites. The RAE decay can be seen in the H- and He-induced x-ray spectra, but background radiation from the heavy-ion atom collision obscures it in the C-N-, and O-induced spectra. The first four members of the KL^n RER satellite sequence $(1s)^{-1}(2p)^{-n}$ to $(2s)^{-2}(2p)^{-n+1}$, which correspond to $n=1$–4, respectively, are observed. The $n=5$ and 6 KL^n RER satellites would occur in a region where the x-ray intensity is dominated by the characteristic $K\alpha$ radiation and therefore is not evident. Similarly the Si K x-ray results are shown in Fig. 6. The effect of the different projectiles on the normal target radiation produces various single-K- and multiple-L-shell vacancy distributions. The variation in the relative intensities of each of the $K\alpha L^n$ satellites should be reflected by a similar variation in the relative intensities of the RER peaks in order that the branching ratios from the initial states $(1s)^{-1}(2p)^{-n}$ to the final states (KL^n RER)$[(2s)^{-2}(2p)^{-n+1}]$ and $K\alpha L^n[(2p)^{-n-1}]$ remain

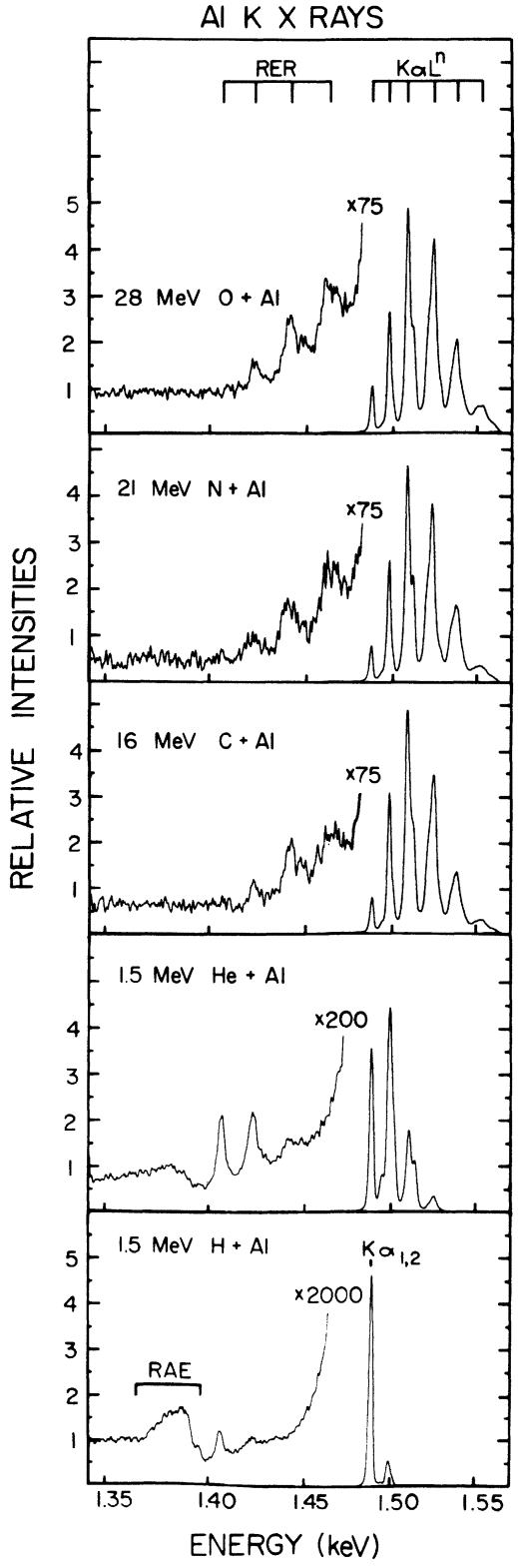

FIG. 5. Al K x-ray spectra produced by O, N, C, He, and H bombardment, showing the relationship between the RER and the $K\alpha L^n$ satellite sequences.

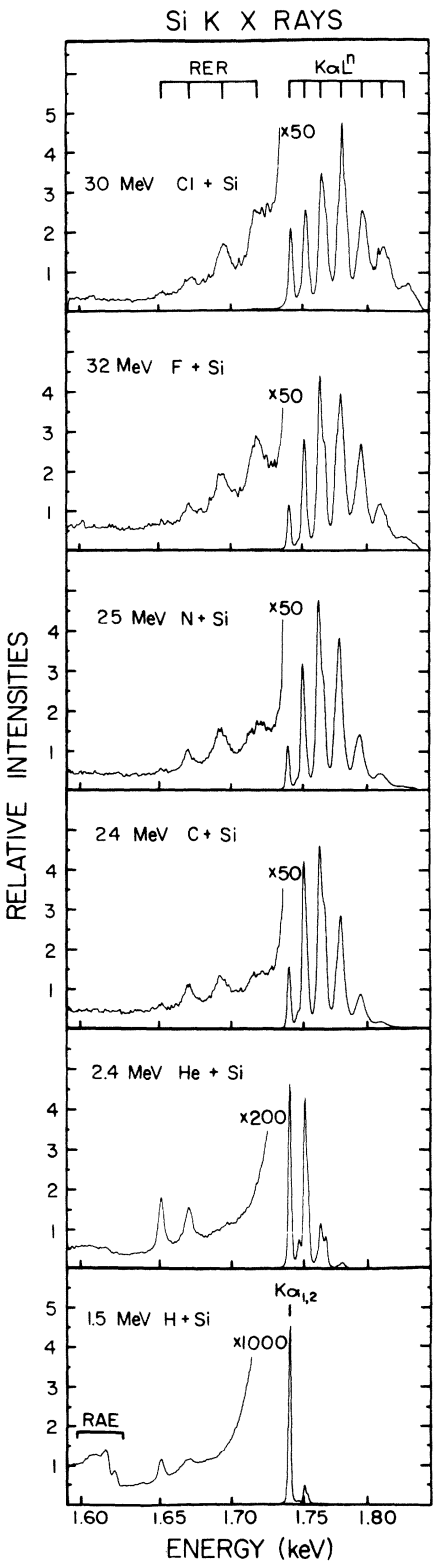

FIG. 6. Si K x-ray intensity produced by Cl, F, N, C, He, and H bombardment shown as a function of energy. The competing decay modes RER and $K\alpha L^n$ are shown for various heavy-ion-produced x-ray spectra.

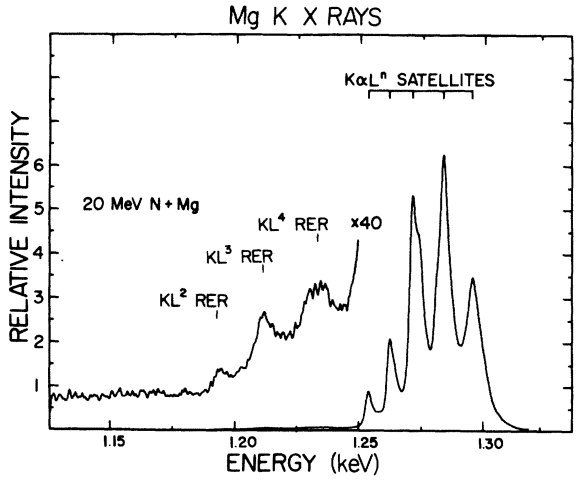

FIG. 7. Second-order Mg K x-rays as analyzed by a TlAP crystal following 20-MeV N bombardment.

constant. Note that $K\alpha_{1,2}$, also denoted as $K\alpha L^0$, has no RER branch, since the initial state has no $2p$ vacancy. Further support for the RER model can be seen in Fig. 7, which shows Mg x rays produced by 20-MeV N bombardment. The Mg x rays were analyzed in second order with a TlAP crystal. Although counting times became quite long when using second-order Bragg diffraction, it is important to show that these peaks are not anomalous first-order crystal effects.

B. Rearrangement transition energies

Table I gives the experiment energies of the RAE edge and the KL^n RER satellites for Mg, Al, and Si. Theoretical energies are given for comparison. The Hartree-Fock computer program of Froese-Fischer[10] was used to calculate the rearrangement transition energies. The calculated energies are normalized to the accepted values of the $K\alpha_{1,2}$ energies, since the Hartree-Fock energies for $K\alpha_{1,2}$ are approximately 0.5% lower than the accepted values. The agreement between experiment and theory is quite good and has been shown to be correct over a larger range of Z (11–22) in a previous publication.[3]

The observed RAE edge energies are compared in Table I to the theoretical $KL_{23}L_{23}(^1D)$ RAE values given by Åberg.[14] It is interesting that while Al and Si show a reasonable spread between KL^1 RER and the RAE edge, the Mg calculations predict KL^1 RER below the RAE edge. These results are consistent with Fig. 3, in which KL^1 RER is masked by the RAE edge. Åberg and Utriainen[15] observe with better energy resolution an anomalous bump on the RAE edge of Mg which can now be attributed to KL^1 RER.

TABLE I. Rearrangement transition energies for Si, Al, and Mg targets.

Target	Produced by	RAE (edge)	KL^1 RER	KL^2 RER	KL^3 RER	KL^4 RER
Si	H^+	1616.0	1650.0	1666.3	...	...
Si	He	1614.5	1649.1	1667.6	...	...
Si	Heavy ion [a]	1613.8	1647.3	1667.2	1690.7	1715.5
Si	Theoretical [b]	1611.1	1646.0	1668.0	1692.0	1718.0
Al	H^+	1392.3	1406.4	1423.4	...	...
Al	He	...	1406.1	1422.6	...	...
Al	Heavy ion [a]	...	...	1422.9	1442.9	1464.1
Al	Theoretical [b]	1393.3	1403.0	1422.0	1444.0	1468.0
Mg	H^+	1181.0	...	...	...	...
Mg	Heavy ion [a]	...	1180.0	1197.0	1215.0	1235.0
Mg	Theoretical [b]	1182.4	1179.0	1196.0	1215.0	1237.0

[a] Energies given in the rows labeled "Heavy ion" are mean values for C-, N-, O-, F-, and Cl-ion bombardment.

[b] Hartree-Fock (see Ref. 10) predicted energies normalized to the characteristic $K\alpha$ energy. The theoretical energy for the RAE edge is taken as the $KL_{23}L_{23}(^1D)$ Auger transition energy (see Ref. 14).

C. Experimental branching ratios

An important aspect of the RER model is the relative intensities of the KL^n RER peaks as produced by various projectiles. The RER model predicts KL^n RER decay rates which are independent of the mechanism which produces the single-K-multiple-L-shell vacancy states. Thus similar

TABLE II. Experimental branching ratios for the various targets, beams, energies, and crystals used in this work.

Target	Beam	Energy (MeV)	Crystal	Branching ratio 10^4B_1	10^4B_2	10^4B_3	10^4B_4
Si	H	1.5	EDdT	16	...	...	...
Si	He	2.4	EDdT	19	58	...	...
Si	C	24	EDdT	20	51	121	313
Si	N	25	EDdT	16	45	120	324
Si	F	32	EDdT	...	53	142	235
Si	Cl	30	EDdT	25	64	105	188
Si	F	20	PET	23	51	152	214
Si	F	25	PET	16	51	151	239
Si	F	30	PET	28	58	159	244
Si	F	35	PET	17	51	144	216
Si	F	40	PET	18	44	157	196
Si	F	45	PET	17	39	135	199
	Average			19.5 ± 4	50 ± 6	137 ± 18	237 ± 47
Al	H	1.5	ADP	15	56	...	...
Al	H	2.0	ADP	17	...	...	...
Al	He	1.5	ADP	16	46	...	...
Al	He	2.0	ADP	16	35	...	...
Al	C	16	ADP	...	...	76	357
Al	O	28	ADP	...	29	89	355
	Average			16 ± 4	41 ± 10	85 ± 21	356 ± 89
Mg	N	20	TlAP	...	37	126	414
Mg	C	20	TlAP	...	32	142	348
	Average				35 ± 8	134 ± 33	381 ± 95

branching ratios of KL^n RER to $K\alpha L^n$ for H through Cl beams would support the RER model. Several factors make the extraction of an experimental branching ratio difficult. Typical counting statistics in the RER portion of the spectra were on the order of 10%. The functional form for the background used to subtract the low-energy tail of the characteristic radiation from the RER peaks produces an additional uncertainty in the relative intensities. In several cases the beam current was reduced just before scanning the characteristic x-ray region, producing an uncertainty in the normalization between the RER and $K\alpha L^n$ portions of these spectra. Considering these factors to be the major sources of error, we estimate the uncertainty in reproduction of the branching ratios to be on the order of 25%.

Table II gives the measured values of the branching ratios for Si. No systematic trends with projectile Z or energy are evident within the experimental uncertainty of ±25%. The average measured branching ratios for Si extracted from all the data are as follows: $(0.195 \pm 0.04)\%$ for $(KL^1$ RER$)/K\alpha L^1$; $(0.50 \pm 0.06)\%$ for $(KL^2$ RER$)/K\alpha L^2$; $(1.37 \pm 0.18)\%$ for $(KL^3$ RER$)/K\alpha L^3$; and $(2.37 \pm 0.47)\%$ for $(KL^4$ RER$)/K\alpha L^4$.

The preliminary values of the branching ratios for Mg obtained by C and N bombardment are 0.35% for $(KL^2$ RER$)/K\alpha L^2$, 1.34% for $(KL^3$ RER$)/K\alpha L^3$, and 3.81% for $(KL^4$ RER$)/K\alpha L^4$. The average values of the branching ratios for Al are 0.16% for $(KL^1$ RER$)/K\alpha L^1$, 0.41% for $(KL^2$ RER$)/K\alpha L^2$, 0.85% for $(KL^3$ RER$)/K\alpha L^3$, and 3.56% for $(KL^4$ RER$)/K\alpha L^4$. Based on the systematics seen in Figs. 5 and 6, more reliable branching ratios could be obtained for these elements using intermediate-Z beams of Li and Be at energies near 2 MeV/amu.

IV. THEORETICAL ESTIMATES

No fundamental selection rule prohibits simultaneous photon and electron emission or photon emission plus double electron rearrangement.[2] One mechanism for radiative electron rearrangement transitions is configuration mixing of the atomic states. A model for RER decay is presented here which uses the electron-electron interaction as the mechanism for the mixing of the final states. Figure 8 shows schematically the possible modes of decay of the $(1s)^{-1}(2p)^{-1}$ initial configuration. This initial configuration, which couples to ^1P and ^3P states, can decay by emission of an $E1$ photon to the $(2p)^{-2}$ final configuration, which couples to three possible multiplet states, ^1S, ^1D, and ^3P. The allowed transitions ^1P-^1S, ^1P-^1D, and ^3P-^3P account for the dominant

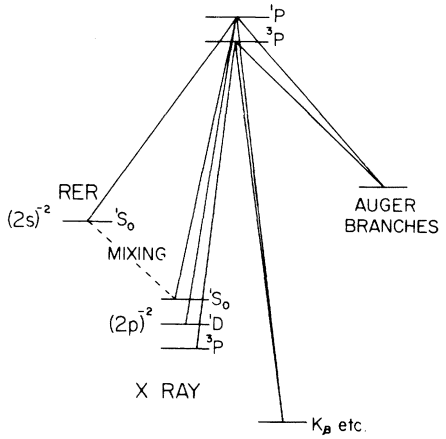

FIG. 8. Schematic diagram of the decay of a single-K, single-L vacancy state shown with the various possible final states. The theoretical branching ratio is calculated for configuration mixing of the two $^1S_0$ levels of the $(2s)^{-2}$ and $(2p)^{-2}$ configurations.

yield in the satellite peak labeled $K\alpha L^1$. It is assumed that the initial configuration $(1s)^{-1}(2s)^{-1}$ results in a small percentage of the $K\alpha L^1$ intensity, and it is neglected. As indicated in Fig. 8, the final configuration $(2s)^{-2}$, which couples to a $^1S_0$ state (ψ_1), will be mixed, by the Coulomb repulsion operator, with the $^1S_0$ state (ψ_2) of the $(2p)^{-2}$ configuration. From energy-difference considerations only these two $^1S_0$ states have significant mixing. New mixed states $\psi_1' = B\psi_1 + A\psi_2$ and $\psi_2' = -A\psi_1 + B\psi_2$ with energy difference ϵ are defined (see Fig. 9). The off-diagonal matrix elements are

$$I = \langle \psi_1 | \sum \frac{e}{r_{ij}} | \psi_2 \rangle = -\frac{1}{\sqrt{3}} G(2p, 2s) , \qquad (1)$$

as outlined by Condon and Shortley[16] and Slater,[17] where G^1 is the Slater exchange integral which is calculated from the Hartree-Fock program of Froese-Fischer.[10] The mixing coefficient A is calculated by diagonalizing the matrix

$$\begin{pmatrix} E_1 & I \\ I & E_2 \end{pmatrix} \psi_k' = E_k' \psi_k' . \qquad (2)$$

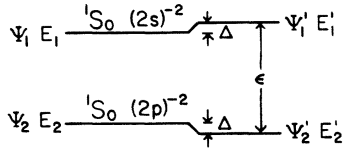

FIG. 9. Schematic diagram of the final-state mixing notation and parameters for the double hole states $(2s)^{-2}$ and $(2p)^{-2}$. $\Psi_1' = B\Psi_1 + A\Psi_2$, $\Psi_2' = -A\Psi_1 + B\Psi_2$, ϵ is the observed energy splitting, and Δ is the theoretical level shift.

TABLE III. Mixing coefficients and branching ratios for Si.

Branch	Initial configuration	$G^1(2p2s)$ (eV)	ϵ (eV)	A^2	F_ω	B.R. Theor.	B.R. Expt.
$(KL^1$ RER)-$K\alpha L^1$	$(1s)^{-1}(2p)^{-1}$	28.59	102	0.026	0.069	0.0018	0.001 95
$(KL^2$ RER)-$K\alpha L^2$	$(1s)^{-1}(2p)^{-2}$	29.29	95	0.021	0.307	0.0065	0.0050
$(KL^3$ RER)-$K\alpha L^3$	$(1s)^{-1}(2p)^{-3}$	29.95	87	...	...	...	0.0137
$(KL^4$ RER)-$K\alpha L^4$	$(1s)^{-1}(2p)^{-4}$	30.57	78	...	...	...	0.0237

A^2 is then given by

$$A^2 = \tfrac{1}{2} - [1/2(E_1' - E_2')][(E_1' - E_2')^2 - 4I^2]^{1/2} . \quad (3)$$

If we let $E_1' - E_2' = \epsilon$ (the experimental energy difference between the KL^n RER and $K\alpha L^n$, as given in Fig. 9) then A^2 reduces to

$$A^2 = \tfrac{1}{2} - \tfrac{1}{2}(1 - 4I^2/\epsilon^2)^{1/2} \sim I^2/\epsilon^2 . \quad (4)$$

The fact that the interaction I^2/ϵ^2 is small gives the leading term of I^2/ϵ^2 in the expansion of the radical in Eq. (4). This yields

$$A^2 = [G^1(2p, 2s)]^2/3\epsilon^2 . \quad (5)$$

The experimental branching ratio is defined as

$$B_E \equiv \frac{KL^1 \text{ RER}}{K\alpha L^1} \simeq \frac{N_x(^1P \rightarrow {}^1S_0(\psi_1'))}{N_x(^1P, {}^3P \rightarrow {}^1S, {}^1D, {}^3P)} . \quad (6)$$

The corresponding theoretical branching ratio calculated from the final-state configuration model is

$$B_T = \frac{A^2 \omega_{1P}(^1S_0)}{\omega_{1P} + 3\omega_{3P} - A^2\omega_{1P}(^1S_0)} , \quad (7)$$

where $\omega_{1P}(^1S_0)$ is the partial multiplet fluorescence yield of the $^1P(1s)^{-1}(2p)^{-1}$ state to the $^1S_0(2p)^{-2}$ state, and ω_{1P} and ω_{3P} are the partial fluorescence yields, respectively, of the $^1P(1s)^{-1}(2p)^{-1}$ state to $^1S(2p)^{-2}$ and $^1D(2p)^{-2}$ states and the $^3P(1s)^{-1}(2p)^{-1}$ state to the $^3P(2p)^{-2}$ state. It is assumed that the initial states are statistically populated, which leads to the factor of 3 in the denominator for the ^3P state. Substituting the expression for A^2 given in Eq. (5) into Eq. (7) yields

$$B_T = \frac{[G_1(2s, 2p)]^2}{3\epsilon^2} \frac{\omega_{1P}(^1S_0)}{\omega_{1P} + 3\omega_{3P}} . \quad (8)$$

The third term in the denominator of Eq. (7) is small compared to the first term and thus neglected. The fluorescence yield factor is referred to as F_ω.

The partial fluorescence yields required to calculate the value of B_T in Eq. (8) are not presently available for Mg, Al, or Si. An estimate of the branching ratio can be made, however, by using the partial multiplet fluorescence yields of Ne calculated by Bhalla.[11] By using the Ne values, the effects of the M-shell electrons in Mg, Al, and Si are not included. This implies that the effects of the $K\beta$ x-ray, KLM Auger, and KMM Auger rates are neglected. However, since the branching ratio depends on the ratio of fluorescence yields, this may not lead to a large error. The value of B_T for KL^1 RER in Si using these assumptions is 0.0018, compared with the measured value B_E of $0.001\,95 \pm 0.0004$. A similar calculation is performed for KL^2 RER of Si, where A^2 is $\frac{2}{9}[G^1(2p, 2s)]^2/\epsilon^2$ and F_ω is 0.307, which yields a B_T of 0.0065, compared with the measured value B_E of 0.0050 ± 0.0006. Table III summarizes the values of G^1, ϵ, A^2, B_T, and B_E for Si. The evaluation of the branching ratios for the third and fourth RER's has not been performed. Many additional calculations of the mixing coefficients, multiplet states, and their partial fluorescence yields are required. Table III shows that with the addition of L-shell vacancies to the initial state the exchange integral increases while the energy separation ϵ decreases. Both factors tend to increase the mixing coefficient and hence the branching ratio. The value of $[G^1(2p, 2s)/\epsilon]^2$ increases by a factor of 2, while the experimental branching ratio increases a factor of 12. Part of this increase is probably due to the fluorescence yield factor. A change of this order of magnitude is not at all unexpected when one examines the dramatic changes in fluorescence yield[11,18] with increased L-shell vacancies.

V. CONCLUSION

We have presented an experimental study of single-photon two-electron rearrangement transitions at energies below the characteristic $K\alpha$ transition. The indentification of the KL^n RER transitions is corroborated by Hartree-Fock calculations for the energies of $(1s)^{-1}(2p)^{-n}$ to $(2s)^{-2}(2p)^{-n+1}$ transitions. Final-state configuration mixing predicts the correct branching ratio

for KL^1 RER and KL^2 RER of Si. Calculations of the partial multiplet fluorescence yields for the targets of Mg, Al, and Si are required to justify more exhaustive calculations of all the branching ratios.

ACKNOWLEDGMENT

The authors wish to give special thanks to Professor Teijo Åberg for many illuminating discussions.

---

*Work supported in part by the U. S. Energy Research and Development Administration under Contract No. E(11-1)-2753.

†Present address: Los Alamos Scientific Laboratory, Los Alamos, N. M.

‡Present address: Bell Laboratories, Murray Hill, N. J.

§On leave from North Texas State University, Denton, Tex.

[1]T. Åberg, Phys. Rev. A 4, 1735 (1971).

[2]T. Åberg, *Atomic Inner-Shell Processes*, edited by B. Crasemann (Academic, New York, 1975), p. 353.

[3]K. A. Jamison, J. M. Hall, and P. Richard, J. Phys. B 8, L458 (1975).

[4]T. Åberg and J. Utriainen, Phys. Rev. Lett. 22, 1346 (1969).

[5]J. Siivola, J. Utriainen, M. Linkoaho, G. Graeffe, and T. Åberg, Phys. Lett. 32A, 438 (1970).

[6]P. Richard, J. Oltjen, K. A. Jamison, R. L. Kauffman, C. W. Woods, and J. M. Hall, Phys. Lett. 54A, 169 (1975).

[7]P. Richard, C. F. Moore, and D. K. Olsen, Phys. Lett. 43A, 519 (1973).

[8]J. McWherter, J. E. Bolger, H. H. Wolter, D. K. Olsen, and C. F. Moore, Phys. Lett. 45A, 57 (1973).

[9]J. Oltjen, R. L. Kauffman, C. W. Woods, J. M. Hall, K. A. Jamison, and P. Richard, Phys. Lett. 55A, 184 (1975).

[10]C. Froese-Fischer, Comput. Phys. Commun. 4, 107 (1972).

[11]C. P. Bhalla, Phys. Rev. A 12, 122 (1975).

[12]D. G. McCrary and P. Richard, Phys. Rev. A 5, 1249 (1972); D. G. McCrary, M. Senglaub, and P. Richard, Phys. Rev. A 6, 263 (1972).

[13]A. R. Knudson, D. J. Nagel, P. G. Burkhalter, and K. T. Dunning, Phys. Rev. Lett. 26, 1149 (1971).

[14]T. Åberg, paper presented at the International Symposium on Electron Spectroscopy, Kiev, 1975 (unpublished).

[15]T. Åberg and J. Utriainen, Solid State Commun. 16, 571 (1975).

[16]E. U. Condon and G. H. Shortley, *The Theory of Atomic Spectra* (Cambridge U.P., London, 1957).

[17]J. C. Slater, *Quantum Theory of Atomic Structure* (McGraw-Hill, New York, 1960), Vols. 1 and 2.

[18]M. H. Chen and B. Crasemann, Phys. Rev. A 12, 959 (1975).